Published in final edited form as:
J Mol Biol. 2006 December 8; 364(4): 716–734.

In Meso Structure of the Cobalamin Transporter, BtuB, at 1.95 Å Resolution

V. Cherezov[4,6], **E. Yamashita**[5,7], **W. Liu**[3], **M. Zhalnina**[5], **WA Cramer**[5], and **M. Caffrey**[1,2,3,4,*]

[1]*Chemical and Environmental Science Department and Materials and Surface Science Institute, University of Limerick, Limerick, Ireland;* [2]*Biochemistry, The Ohio State University, Columbus, OH 43210, USA* [3]*Biophysics, The Ohio State University, Columbus, OH 43210, USA* [4]*Chemistry, The Ohio State University, Columbus, OH 43210, USA* [5]*Department of Biological Sciences, Purdue University, West Lafayette, IN 47907, USA*

Summary

Crystals of the apo-form of the vitamin B_{12} and colicin transporter, BtuB, that diffract to 1.95 Å have been grown by the membrane-based *in meso* technique. The structure of the protein differs in several details from that of its counterpart grown by the more traditional, detergent-based (*in surfo*) method. Some of these differences include i) the five N-terminal residues are resolved *in meso*, ii) residues 57–62 in the hatch domain and residues 574–581 in loop 21–22 are disordered *in meso* and are ordered *in surfo*, iii) residues 278–287 in loop 7–8 are resolved *in meso*, iv) residues 324–331 in loop 9–10, 396–411 in loop 13–14, 442–458 in loop 15–16 and 526–541 in loop 19–20 have large differences in position between the two crystal forms, as have residues 86–96 in the hatch domain, and v) the conformation of residues 6 and 7 in the Ton box (considered critical to signal transduction and substrate transport) are entirely different in the two structures. Importantly, the *in meso* orientation of residues 6 and 7 is similar to that of the vitamin B_{12}-charged state. These data suggest that the 'substrate-induced' 180-degree rotation of residues 6 and 7 reported in the literature may not be a unique signaling event. The extent to which these findings agree with structural, dynamic and functional insights gleaned from site-directed spin labeling and electron paramagnetic resonance measurements is evaluated. Packing in *in meso*-grown crystals is dense and layered, consistent with the current model for crystallogenesis of membrane proteins in lipidic mesophases. Layered packing has been used to locate the transmembrane hydrophobic surface of the protein. Generally, this is consistent with tryptophan, tyrosine, lipid and C_α-B-factor distributions in the protein, and with predictions based on transfer free energy calculations.

Keywords

Colicin; Cubic phase; Membrane protein crystals; Vitamin B_{12}; X-ray diffraction

*__Corresponding author:__ M. Cafffey, E-mail: martin.caffrey@ul.ie.
[6]Current address: Department of Molecular Biology, The Scripps Research Institute, La Jolla, CA 92037, USA
[7]Current address: Institute for Protein Research, Osaka University, 3–2 Yamadaoka, Suita-shi, Osaka, Japan.

INTRODUCTION

In gram-negative bacteria, uptake of essential nutrients such as cyanocobalamin (CNCbl, Vitamin B_{12}) and iron complexes involves a family of outer membrane transport proteins that begin the process by concentrating their respective substrates in the periplasmic space. In *Escherichia coli* this so-called TonB-dependent transport (TBDT) family includes BtuB, which is responsible for CNCbl uptake and FepA, FecA, and FhuA for importing iron in different forms. CNCbl is an important cofactor in the metabolism of amino acids and nucleotides. In humans, deficiencies lead to pernicious anaemia. It is a medium sized (M_r 1,355 g/mol), water-soluble molecule built around a cobalt ion coordinated to 4 pyrrole nitrogens from a corin porphyrin, a dimethylbenzimidazole ribonucleotide and a cyano group. The ability of many of the A-type colicins to utilize BtuB as their receptor for entry through the outer membrane[1,2] is an example of the ability of colicins and phages to parasitize outer membrane transport proteins for their own entry.

The movement of CNCbl from the extracellular medium into the cytosol of *E. coli* involves several participants, the first of which is BtuB, a 22-stranded antiparallel β-barrel protein that spans the outer membrane. While the detailed mechanism of transport into the cytosol is not known, certain aspects of the process have been elucidated. For example, BtuB has been shown to bind CNCbl from the extracellular medium with very high affinity. Subsequently, the vitamin is transferred through the periplasm and across the inner membrane in an energy-dependent process that is coupled to the proton motive force across the cytoplasmic membrane. A trans-periplasmic protein, TonB, which is anchored in the inner membrane interacts functionally with the inner membrane proteins ExbB and ExbD. An energized form of TonB is presumed to associate with BtuB in its substrate-loaded form to facilitate import and release of CNCbl into the periplasm.

The structure of BtuB solved with and without CNCbl sheds some light on how the protein functions to move substrate across the outer membrane.[3] It is a β-barrel, 594 residues long that spans the membrane. The lumen of the barrel is approximately elliptical in shape with major and minor axes measuring 42 Å and 37 Å, respectively. Its maximum height is 55 Å. The protein has a hatch or plug domain of 127 residues, extending from residue 6–132, tethered to the barrel by a run of four (133–136) amino acids – the so-called linker region. The hatch domain sits in and fills the lumen, effectively blocking the barrel pore. The substrate binds to the extracellular surface of the hatch domain. It is assumed that binding triggers a series of events leading to ligand movement from the extracellular side of the outer membrane and into the periplasm. However, the details of this triggering action are unclear, as are the mechanisms of transfer of vitamin B_{12} and colicin across the outer membrane.

How is the substrate-charged status of the BtuB protein communicated to downstream partners in the transport system, most immediately TonB? The TBDTs all possess a highly conserved amino acid sequence, the Ton box, of form A-Thr-H-H-Val-H-Ala where A and H generally are acidic and hydrophobic residues, respectively. The Ton box is located toward the N-terminus of the TBDT. It is assumed to interact with the TonB protein upon substrate loading in a way that sets in motion movement of substrate from the extracellular side of the transporter into the periplasm. The structure study of Chimento et al.[3] showed that a well-defined change in the Ton box region of BtuB accompanied substrate binding. In BtuB, the Ton box includes residues 6 through 12, and a 180-degree rotation of residues 6 and 7 was reported to take place on substrate binding. Based on these findings, it was proposed that this represented the “first direct structural determination of the transmembrane signaling that occurs in the Ton box of a TonB-dependent transporter upon binding of its substrate”.[3] However, the flip undergone by residues 6 and 7 upon substrate binding left them in the same plane on the periplasmic surface of the hatch domain as in the apo-form. It might have been expected that the apo or holo-forms

of the protein would have the Ton box, or parts thereof, extend out and away from the hatch periplasmic surface for association with the TonB protein. The interpretation was made somewhat more difficult by the absence of structure for the five residues N-terminal to the Ton box which were disordered in the presence and absence of substrate.

A considerable body of information has been gathered on the structure and dynamics of the N-terminal region of BtuB using site-directed spin labeling (SDSL) and electron paramagnetic resonance (EPR).[4–6] Upon substrate binding, the Ton box underwent what was interpreted to be a change from a folded to an unfolded conformation. Additionally, residues C- and N-terminal to the Ton box had increased mobility upon ligand binding. Because little change took place in the mobility of residues 16 and 17, it was felt that these represented a hinge about which the rest of the N-terminus moved on substrate binding. These, so-called docking and undocking events were observed to take place in intact outer membranes and in purified BtuB protein reconstituted into bilayered phospholipid vesicles.

The crystallographic and EPR studies are obviously at variance. The former shows a substrate-induced change in the conformation of two Ton box residues that remain tucked in close to the periplasmic surface of the hatch domain. In contrast, the EPR work suggests a dramatic unfolding and a pulling away from the hatch domain of the N-terminus upon substrate binding. However, both techniques are prone to artifacts, as noted.[4]

We have been interested in the BtuB system from several perspectives, some of which have to do with membrane protein crystallogenesis by the *in meso* method for structure determination.[7,8] Thus far, the method has had success mostly with chromophore-containing α-helical proteins that include bacteriorhodopsin, halorhodopsin, sensory rhodopsin with and without a transducer fragment, the light harvesting complex 2 (LH2) and the bacterial photosynthetic reaction center (http://www.lipidat.chemistry.ohio-state.edu/MPDB/index.asp). In preliminary studies, we had demonstrated that it was possible to crystallize apo-BtuB which was the first non-chromophore containing β-barrel protein to have yielded to the *in meso* method.[9] However, the crystals diffracted only to 4 Å. Accordingly, part of the current study was to optimize the method with a view to growing crystals of significantly better diffraction quality.

Fanucci et al.[5] have commented that the N-terminus of BtuB, which includes the Ton box, unfolds in detergent micelles. It refolds when the protein is reconstituted into bilayers. The crystallographic work on BtuB by Chimento et al.[3,10] was done with crystals grown using mixed protein/surfactant micelles by the so-called *in surfo* method.[8] In contrast, the EPR measurements were done in lipid bilayers. It is possible therefore that the disparities highlighted above and elsewhere[5] in regard to the signaling mechanism can be attributed, at least in part, to the medium in which the protein was dispersed – micelles *versus* bilayers. Further, the lack of order in the first five N-terminal residues of the BtuB model[3] could be ascribed to the micellar environment used for crystal growth. In contrast, the *in meso* method employs lipid bilayers as the medium in or from which crystals grow. It was considered worthwhile therefore to evaluate this alternative approach for structure determination since the prospect was that it would support order in the N-terminal region of the substrate-free protein. Additionally, considerable disorder was observed in some of the extracellular loops connecting adjacent strands of the β-barrel in the *in surfo*-grown crystals.[3] The hope was that the alternative, bilayer-based *in meso* method would produce crystals with well-defined loops, if indeed they are naturally ordered.

One additional issue that was of interest concerned the packing density of *in meso*-grown crystals. The structure of LH2 has been solved using crystals grown *in surfo* and *in meso* and the latter have a packing density almost twice that of the former.[11] This has been explained

by the manner in which crystals form *in meso* which allows for close, side-by-side packing of proteins. In contrast, *in surfo*-grown crystals often have a band of detergent encircling the protein that can work against direct, side-by-side contact. The generality of these observations is examined in this study.

RESULTS

Preliminary Characterization

As noted in the Introduction, the *in meso* method begins with what is assumed to be a reconstitution of the protein into the lipid bilayer of the cubic phase. In what follows, evidence in support of this assumption is provided. To begin with, the protein is combined with the lipid, monoolein, in a ratio that should produce the cubic phase provided the detergent concentration of the protein solution is not too high.[12] When this was done with the BtuB preparation, the cubic-Pn3m phase was produced as evidenced by small-angle X-ray diffraction (Figure 1(b)). The lattice parameter of the cubic phase was 104.3 Å, which is similar to the value observed with a control monoolein/water sample (104.8 Å). Upon addition of precipitant solution to trigger nucleation and crystal growth, the cubic phase swelled and formed what is referred to as a sponge phase (Figure 1(c)), as observed previously.[11] It is from this swollen, bicontinuous mesophase that the crystals of BtuB were harvested.

Spectroscopic measurements were made to determine the state of the protein while reconstituted in the cubic phase. The UV-visible spectra of the BtuB preparation in micellar form and *in meso* are shown in Figure 2(a). Within experimental error, the spectral properties are the same regardless of the protein dispersion state. CD spectra showed that the gross secondary structure was insensitive to whether the protein was in a micellar or a bilayer environment (Figure 2(b)).

Quenching of tryptophan fluorescence by a lipid with a dibrominated acyl chain (bromo-MAG) has been used to demonstrate reconstitution of gramicidin in the lipidic mesophase.[13] This same approach was employed with BtuB and the data are shown in Figure 2(c). BtuB has 13 tryptophans (Figure 3(a)), 12 of which should be accessible to quenching by bromo-MAG provided the protein is reconstituted into the lipid bilayer of the cubic phase. The extent of quenching observed (> 80 %) is consistent with this expectation (Figure 2(c)) and supports the view that BtuB is reconstituted prior to crystallization.

We also wished to determine whether or not the protein retained 'functionality' *in meso* prior to crystallization. This was examined by measuring CNCbl binding to BtuB reconstituted into the cubic phase. Control samples that lacked the protein exhibited no binding while test *in meso* BtuB-containing samples showed convincing evidence of substrate uptake (Figure 2(d) and (e)). Binding was shown by quenching of intrinsic fluorescence of aromatic residues by CNCbl to be extremely tight with a dissociation constant, K_d, of ~1 nM (Figure 2(d)). Similar K_d's have been reported for the native membrane-bound14 and micellarized form of the protein.[15] Interestingly, in the absence of added calcium no evidence was found for ligand binding to cubicized BtuB (data not shown).

Taken together, these data support the view that the protein reconstitutes into the bilayer of the cubic phase in an active form prior to *in meso* crystallization.

Molecular Structure

The structure of apo-BtuB has been determined to 1.95 Å resolution with crystals grown *in meso*. The general features of the protein are very similar to those reported for substrate-free BtuB crystals produced by the traditional *in surfo* method[3] with a backbone root mean square deviation (RMSD) of 2.87 Å. Despite the similarities, there are important differences that will

be discussed below. The N-terminus, extending through the Ton box and the hatch domain, is resolved in the *in meso* structure. The five residues, 1Q-D-T-S-P5, N-terminal to the Ton box, 6D-T-L-V-V-T-A12, are directed away from the periplasm, with residue Q1 contacting the periplasmic edge of the 4-stranded β-sheet that forms the hydrophobic core of the hatch domain. All features of the hatch domain are clearly seen with the exception of the first substrate binding loop, SB1, extending from residues 57 to 62 which are disordered in the *in meso* structure. The other two substrate-binding loops and the linker region that tethers the hatch domain to the β–barrel are well defined. All 22 strands of the β–barrel are resolved, as are the 10 short turns that connect adjacent strands at the relatively flat periplasmic extremity of the protein. Of the 11 relatively lengthy loops that connect adjacent β–barrel strands, 8 are clearly visible and 3 are disordered.

The *in meso* apo-BtuB structure includes 11 long chain molecules that have been identified as monoolein. Each has a chain 18 carbon atoms long with a polar headgroup composed of 3 carbon and 3 oxygen atoms which presumably represent glycerol. A high temperature factor precludes identification of the acyl carbonyl oxygen and the double bond between carbon atoms 9 and 10 in the acyl chain. The protein was purified in LDAO, a detergent with an acyl chain 12 carbon atoms long. However, there are no such molecules in the solved structure, which is not unreasonable given the vast molar excess of lipid over detergent that is used in *in meso* crystallogenesis.[8]

In addition to the lipid, the model includes four molecules of MPD and one of formate which is consistent with the fact that the crystallization precipitant contained 10 %(v/v) MPD and 0.2 M ammonium formate. 297 water molecules are associated with the structure. There is no indication that the protein has any associated ions or substrate molecules. Given that the sample was prepared in the absence of added substrate, and with EDTA, which will strip the protein of calcium, and thus CNCbl, this result is not surprising.[14]

As noted, the structure of BtuB determined using *in meso*–grown crystals is, in general, very similar to that of the apo-protein solved using the *in surfo* approach. A comparison of backbone RMSD's for related structures, that include apo-BtuB grown *in meso* and *in surfo*, and the calcium-, calcium/CNCbl- and colicin (R135 fragment)-bound forms all grown *in surfo*, is shown in Table 1. The differences are remarkably small at < 2.9 Å given that the protein is almost 600 residues long with extensive loops on the extracellular side of the barrel that are expected to have considerable flexibility. However, the RMSD is an average value over the entire structure and it masks large differences that are apparent in select parts of the protein, as summarized below: 1) the five N-terminal residues are resolved *in meso*, 2) residues 57–62 in the hatch domain and residues 574–581 in loop 21–22 are disordered *in meso*, but ordered *in surfo*, 3) residues 278–287 in loop 7–8 are resolved *in meso*, 4) residues 324–331 in loop 9–10, 396–411 in loop 13–14, 442–458 in loop 15–16 and 526–541 in loop 19–20, and residues 86–96 in the hatch domain have different positions in the two crystal forms, and 5) the conformation of residues 6 and 7 in the Ton box are completely different. Thus, based on the *in meso* structure of apo-BtuB, some of the structure changes previously noted that are caused by the binding of cobalamin[3], or of the colicin receptor binding domain, R135[16], are different. Cobalamin binding causes a smaller change of order in the loop 7–8. Of the structure changes caused by binding of the colicin E3 R135 domain, (a) the increase of order of the loop 7–8 is smaller than previously calculated relative to the *in surfo* structure, and the position of the loop 19–20 is changed.

B–factor Distribution

The B-factor, also known as the temperature- or Debye-Waller factor, provides information about the dynamic and static mobility of a structure determined by X-ray diffraction.[17] It is a

measure of the degree to which electrons in atoms or groups of atoms are spread out. It can also reflect errors in model building

A plot of the C_α-B-factor as a function of residue position in the BtuB protein is shown in Figure 4 (red line). A color-coded representation of the C_α-B-factor superimposed on the cartoon model of the isolated barrel and hatch domains is shown in Figure 5. Clearly, the mobility characteristics of the protein, as reflected in the absolute C_α-B-factor values, are lowest in the transmembranal regions of the staves or β-strands of the barrel domain. Here, B-factors range from 21.8 to 49.3 $Å^2$ with an average value of 31.0 $Å^2$. However, the temperature-factor is not uniform for all β-strands in the barrel. Rather, it is particularly low toward one half of the barrel in strands β8 to β17. It then rises to a maximum of 38.2 to 43.7 $Å^2$ where the two 'sides' of the barrel meet along strands β1 and β22, which happen to be two of the shortest strands in the barrel. Generally, the B-factor is slightly higher in the short periplasmic turns that connect β-barrel strands than in the strands themselves. There is one exception in turn 14–15 where the B-factor remains low at < 24 $Å^2$ through the turn. On the opposite end of the barrel, loops connecting barrel strands, which vary from 3 to 21 residues long (average 12 residues), have B-factors that change dramatically depending on location. For some (loops 7–8 and 11–12), the B-factor is low (< 31.6 $Å^2$) while for others (loops 9–10 and 19–20) it reaches values of 61.4 $Å^2$ corresponding to some of the highest temperature-factors found anywhere in the model. It is interesting that in the latter two cases the loops are long and incorporate elements of secondary structure; a β-sheet in loop 9–10 and a helical turn in loop 19–20. Of note is the fact that the B-factor of strands leading into loops 3–4, 5–6 and 21–22, which are disordered and are not seen in the model, all rise in the direction of the missing loops.

The B-factors of the C_α-backbone in the hatch domain have values that, on average (31.7 $Å^2$), are slightly higher than that of the transmembranal strands in the barrel (31.0 $Å^2$). This average holds true for the hydrophobic β-sheet core and for most of the helical stretches in the hatch domain. However, higher values are seen in the region of linkage between the hatch and barrel domains (52.1 $Å^2$) and in residues leading into and out of the substrate binding loop SB-1 (51.0 $Å^2$). The highest B-factors in the entire BtuB model are associated with the protein's first five residues that are immediately N-terminal to the Ton box. Here, values range from 63 to 66 $Å^2$.

The B-factors associated with the lipids show a tendency to rise along the length of the chain in the direction up to and including the headgroup.

DISCUSSION

Crystals of the vitamin B_{12} transporter, BtuB, diffracting to 1.95 Å, have been grown by the membrane-based *in meso* technique. This represents the highest resolution for a β–barrel protein with more than 16 transmembrane strands (http://www.lipidat.chemistry.ohio-state.edu/MPDB/index.asp). It also is the highest resolution for a membrane protein other than bacterial rhodopsin, whose structure has been solved with *in meso*-grown crystals. In the course of this work, we have demonstrated that the protein is reconstituted in an active form into the bilayer of the cubic phase as a preliminary to nucleation and crystal growth. In the following, the significant differences between the *in meso* structure and that solved using more traditional *in surfo* techniques are discussed. The degree to which the current findings agree with structural, dynamic and functional insights gleaned from EPR measurements are evaluated. Finally, the use of the crystal structure to define the location of the protein in its natural membrane environment is described.

Comparison with Known Structures

The Protein—Comparisons will be made between the current *in meso* structure for apo-BtuB and that of its counterpart crystallized using the detergent-based *in surfo* technique.[3,16] Throughout the discussion, reference will be made to Figure 4 in which the sequence, conserved residues, structural features and substrate binding residues are identified along with a plot of the C_α-B-factor and backbone RMSD between the two structures as a function of residue number.

One of the most significant differences between the two structures is in the N-terminal region where the first five residues, missing in the *in surfo* model, are resolved in the *in meso* model. There are five additional regions of the protein where structural comparisons cannot be made. One of these, in the loop between β–barrel strands β7 and β8 (loop 7–8), arises because the segment is disordered in the *in surfo* model. This loop participates in a protein-protein contact *in meso* (Figure 6(b)). The remaining four, in three β–barrel loops (loops 3–4, 5–6, 21–22) and in the first substrate binding loop of the hatch domain (SB-1), come about because of disorder in the corresponding regions of the *in meso* structure.

Where there is common structure, the comparison shows that the bulk of the two proteins are remarkably similar with 82 % (437/533) of the residues having backbone RMSD values of less than 1.5 Å. This is particularly true in the β–strand region of the barrel. There is one notable exception along the extracellular half of strands β15 and β16 which extends into loop 15–16 and which is in a very different location in the two models. In the *in meso* structure, the loop crosses the top of the hatch domain to the center of the barrel lumen, in a way that may block access to the substrate docking site. In contrast, the stems of this loop in the *in surfo* model are almost an extension to the corresponding barrel β-strands with a slight tilting of the loop to the lumen side. This represents the biggest disparity between the two structures where the RMSD value reaches a maximum of 18 Å. Extracellular loops 9–10, 13–14, and 19–20 also show large differences with maximum deviations of ≥ 9 Å. In the first of these, the loops have diametrically opposite directionality. It points away from the barrel center in the *in meso* model and toward it in the *in surfo* form (Figure 7). Loop 13–14 behaves in the same way as loop 15–16 in that it extends into the barrel toward the hatch in the *in meso* model while it is a simple extension of the barrel wall in the *in surfo* structure. In the former, it may contribute, along with loop 15–16 and SB-3, to blocking the substrate binding site. Loop 19–20 is involved in a protein-protein contact in the *in meso* model. There are additional differences, but of lesser magnitude (RMSD, 2 – 5 Å), associated with substrate binding loops SB-2 and SB-3 in the hatch domain. Finally, small deviations, of magnitude 0.6 – 3 Å, are seen with regularity in the RMSD plot that correspond to short turns on the periplasmic side of the protein.

One particularly notable difference between the *in meso* and *in surfo* structures of the apo-BtuB protein is that in the apo-BtuB, the first 5 residues can be seen *in meso* but not *in surfo*. One further disparity is displayed in the first two residues, Asp6-Thr7, of the Ton box, where the C_α-backbones diverge at an angle close to 180 degrees (Figure 8). This difference is reminiscent of the conformational change described by Chimento et al.[3] as the key signaling event associated with substrate binding and signal transduction across the membrane. A comparison between the current *in meso* model for the apo-form of the protein and its *in surfo* counterpart in the calcium/CNCbl-bound form is shown in Figure 8(b). The two are very similar. However, one is with, while the other is without substrate. This result suggests that the 'flipped' conformation of the first two Ton box residues is accessible with and without substrate and that some other conformational change constitutes the signaling event. It is interesting to note that the conformation of these two residues in the BtuB–R135 complex[16] are virtually superimposable on those for the *in meso* model (Figure 9) where neither have substrate bound. These data suggest that the flipped conformation referred to by Chimento et al.[3] is not uniquely associated with the TonB signaling event.

In addition to differences in the Ton box region, there are RMSD's ranging from 2.9 to 5.3 Å in substrate binding loops SB-2 and SB-3 (Figure 9). In the *in meso* model, both loops are rotated in the same direction with respect to their *in surfo* counterparts which is away from the extracellular medium. As noted, the terminus of the SB-1 loop is missing in the *in meso* structure. However, the stem, which is visible, is rotated in the same general direction as seen with SB-2 and SB-3 when the two crystals forms are compared.

While the current work was in review, the structure of holo-BtuB complexed with a C-terminal fragment (residues 147 to 239) of TonB at 2.1 Å resolution was published.[18] Association involves the extension of a 3-stranded β-sheet in the isolated TonB fragment to a 4-stranded sheet in the complex. Ton-box residues 6 through 11 of the substrate-charged BtuB provide the additional strand. In the apo-form of the protein, the Ton box resides within the lumen of the barrel tucked in close to the periplasmic surface of the plug domain. In the complex however, the entire box stretches out and away from the planar base of the barrel at a 45-degree angle in the direction of the periplasm where it engages TonB. (Interestingly, the N-terminal tetrapeptide of BtuB is disordered in the complex. There are also a number of small but significant differences in the loop and hatch regions that will be discussed elsewhere.) Accompanying this movement is an unfolding of a run of peptide (residues 12 through 22) in BtuB that enables the Ton box to reach out from inside the barrel and to contact its downstream partner. Thus, TonB is bound by the N-terminal peptide of BtuB as if locked in place by a bent arm; the forearm includes the Ton box, residues 12 through 22 form the upper arm and Leu22 sits at the shoulder joint. Similar observations have been reported for the FhuA-TonB complex[19] corroborating the results obtained with BtuB-TonB.

Lipids/Detergents/Ions—The crystal structure of the apo-form of BtuB solved by the *in surfo* method (1NQE) contained seven detergent molecules modeled as (hydroxyethyloxy)tri (ethyloxy)octane. This is the non-ionic C_8E_4 detergent that was employed in the final stages of protein purification. A single magnesium ion was also modeled consistent with the fact that magnesium acetate was used in the crystallization precipitant and cyrobuffer solutions.[10] In the case of the *in meso* structure, the non-proteinaceous material other than water included 11 monoacylglycerols, 4 MPD molecules and 1 molecule of formate. There was no evidence for substrate, calcium or magnesium which is reasonable given that protein purification was carried out in the presence of EDTA, as noted.[1]

The lipids in the *in meso* structure are arranged around the membrane-embedded periphery of the BtuB protein in a physico-chemically reasonable way for the most part. Of the eleven lipid molecules, a group of five is on the extracellular side of the protein while a separate group of five is on the periplasmic half corresponding approximately to the two monolayers constituting the lipid bilayer from which the crystals grow. In both groups, the headgroup is aligned toward the putative polar/apolar interfaces of the protein while the chains drape over the outer hydrophobic surface of the barrel. Interestingly, the long axes of the acyl chains tend to be oriented at right angles to the direction of the β–strands in the barrel. Further, the lipid chains from the periplasmic and extracellular sides of the protein interdigitate across the hydrophobic mid-plane of the protein. This is reasonable given that the lipid bilayer in the cubic-Pn3m phase used for *in meso* crystallization is ~35 Å wide[20] while the hydrophobic thickness of the protein is 21.1 Å (http://opm.phar.umich.edu/). The last of the eleven lipid molecules is curiously located on the barrel outer surface essentially where the mid-plane of the bilayer is likely to be.

Halorhodopsin (1E12,21) is the only other membrane protein whose structure has been solved using *in meso*-grown crystals that includes monoolein as bound lipid. In this case, ten molecules were found, nine of which are located aggregated together on the periplasmic half of this α-

helical protein. The remaining lipid molecule is toward the cytoplasmic side of the protein with some interdigitation between chains from the two lipid groups.

Crystal Packing

Packing is very different in *in surfo* and *in meso*-grown crystals of the apo-BtuB protein (Figure 6). The latter show the characteristic layered packing with protein molecules arranged in planar sheets. Nearest neighbors within a layer have opposite polar orientation. When layers are viewed from the side, a continuous band of protein 21 – 23 Å wide is observed that is created by the overlap of adjacent protein molecules within a given sheet. Interaction between proteins within a layer happens as a result of direct barrel-to-barrel contact; specifically, residues in strands β8 through β11 of one protein molecule make contact with residues in strands β14 through β19 of a neighboring molecule. It also comes about indirectly by lipid mediation. Sheet stacking is stabilized by direct protein-protein interaction involving the following contacts: loop 7–8 to loops 11–12 and 13–14, loop 9–10 to loops 15–16 and 17–18, loop 19–20 to turn 20–21 and residue 594 (Figure 6(b)).

In surfo crystal packing is more complicated than the simple, layered arrangement seen with *in meso*–grown crystals. In the former case, direct contact is observed between strands of neighboring β-barrels. These involve stands β8-β11 and β14-β15 (Figure 6(c)). Additionally, indirect contact mediated by detergent is seen where barrels of adjacent protein molecules approach one another (Figure 6(c)). Contact involving turns 2–3 and 18–19 also contribute to creating an ordered lattice in *in surfo*-grown crystals (Figure 6(c)). Packing is also stabilized by a magnesium ion that bridges loop 15–16 of one protein and the strands β2 and β3 of an adjacent protein. Three imidazoles (His174, 176 and 449) are in close proximity (≤2.4 Å) to the magnesium ion. Additional interaction involves loop 19–20 of one protein and strands β4-β7 of another. Interestingly, the loop/β-strand contact points are just outside the proposed apolar transbilayer surface of the barrel.

Crystal Packing Density—The crystal volume per unit protein mass (V_m) for apo-BtuB in *in meso*-grown crystals is 2.62 $Å^3$/Dalton. This translates to a solvent content of 53 % and is consistent with close packing of protein molecules in the crystal. Such low V_m values are commonly encountered with soluble proteins. It would appear to be a characteristic too of membrane proteins that have been crystallized by the *in meso* method where intimate contact between proteins is possible as a result of transport afforded within the hosting mesophase (see below). In contrast, *in surfo*-grown crystals tend to have a higher 'solvent' content, a sizable fraction of which is made up of bound detergent which can work against close packing. Thus, the respective V_m and solvent content values for *in surfo*-grown crystals of apo-BtuB are 3.04 $Å^3$/Da and 60 %. While bigger than the values observed with their *in meso* counterparts, they are on the low side for their class. For comparison, values of 5.2 $Å^3$/Da and 76 % have been reported for the bacterial photosynthetic reaction center (1RZH;22) crystallized by the *in surfo* method.

B–factor

A comparison of the B-factor and how it changes with residue number along the length of the protein in *in meso*- and *in surfo*-grown crystals has been made (data not shown). The most obvious difference between the two profiles is the average B-factor, 33.4 $Å^2$ and 38.1 $Å^2$, for the *in meso* and *in surfo* models, respectively. Neglecting possible contributions from model building errors, these data suggest that the latter has more mobility than the former. This presumably reflects the lower packing density observed in the *in surfo*-grown crystals where typically a sizable fraction of the crystal is made up of ‘fluid’ detergent micelles. In contrast, *in meso*-grown crystals have a high packing density. The more intimate protein-protein contact and the absence of a less structured micellar torus in the crystal likely contribute to the lower

temperature-factor and to reduced protein flexibility. In this regard it is interesting to note that molecular dynamics simulations of the 8-stranded β-barrel portion of OmpA exhibits higher structural fluctuations by a factor of 1.5 in micelles as opposed to lipid bilayers.[23] However, the effect is not completely general in that the average B-factor observed for LH2 *in meso* and *in surfo* is 31 and 23 $Å^2$, respectively (Table 2).

Despite the difference in average B-factor just noted there are similarities between the two models where peaks and troughs in B-factor values as a function of residue number follow one another (data not shown). However, there are regions in the structure where the B-factor values are profoundly different with the *in meso* model having very low mobility characteristics by comparison. These stretches include residues that are associated with hα1 and hα2 (residues 35–45) and SB-3 (residues 81–102) of the hatch domain, the linker (residues 133–139) and strand-loop combinations β2/β3 (residues 154–172), β7/β8 (residues 272–302) and β20/β21 (residues 551–565) in the barrel.

Comparison with SDSL/EPR Work

An impressive array of studies have been performed on BtuB using SDSL and EPR for the purpose of understanding how it moves CNCbl across the outer membrane.[4–6] Typically, measurements involve first mutating the protein in a site-specific manner, replacing the targeted residue with cysteine which is subsequently derivatized with a nitroxide spin label probe. The EPR signal from the label is interpreted to provide information on probe mobility with a view to learning about the motional properties of the corresponding site in the protein.

The primary focus of this body of work has been on the N-terminus of BtuB that includes the Ton box and residues adjacent it. The data have been interpreted as indicating that the Ton box is relatively immobile and in close contact with other parts of the protein in the substrate-free form. In this the so-called ‘docked’ state, residues N-terminal to the Ton box are quite mobile by comparison and are referred to by the authors as being ‘natively disordered’.[4] Residues C-terminal to the Ton box, like the box itself, are relatively immobile in the absence of substrate. Upon ligand binding, the mobility of the entire N-terminus, extending through the Ton box and up to residue 15 or thereabouts, increases. The hinge about which 'undocking' occurs has been located at residues 16 and 17. The sense is that when CNCbl locks into the binding site on the hatch domain the N-terminal pentadecapeptide pulls or is forced away from the body of the protein. This stretch of amino acids presumably now has the mobility to enable the Ton box segment to extend toward the periplasm where it engages with TonB, its downstream partner in the signaling/transport process.

The structure of BtuB solved using *in meso*-grown crystals is consistent to a degree with the picture emerging from the EPR studies. The Ton box and residues 13 through 17 are all ordered and the Ton box has contact with other parts of the protein in its ligand-free form. However, the pentapeptide N-terminal to the Ton box is well defined and ordered in the *in meso* model, despite the fact that its C_α-B–factor is higher than anywhere else in the protein (Figure 4). This is in distinct contrast to the EPR result where the latter segment was found to be intrinsically disordered. Indeed, separate spin labeling studies demonstrated that this N-terminal fragment resisted ordering even in the presence of osmolytes of the type used in crystallization precipitant solutions.[4] Accordingly, the authors of the EPR study described the N-terminal pentapeptide as being ‘natively disordered.’ Support for this characterization came from the *in surfo* crystal structure where the same five residues were not seen in either the ligand-free or ligand-bound form of the protein.[3]

To what then can we attribute the disparity between our result regarding the N-terminal pentapeptide and that of the EPR study? The two methods are entirely different and use very different protein dispersions. However, they both share the common feature of a lipid bilayer

at least initially hosting the protein. As pointed out previously, the crystallographic method can suffer from issues having to do with osmotically trapped intermediate states[4] and crystal packing forces.[24] On the other hand, the EPR technique relies upon the use of a mutation coupled with chemical labeling both of which can be perturbing[4,25]. In fact, when the spin label is suitably positioned in the Ton box it creates disorder reminiscent of the undocking event that occurs on ligand binding. It is possible therefore that the interpretation given for the EPR results simply reflects the chemical change that goes along with site directed spin labeling. It is important to appreciate too that the EPR technique reports on mobility, a quantity that combines rate and amplitude of motion. In the studies under discussion no attempt was made to separate the two contributions. Thus, a change in mobility, as reflected in a change in the breadth of the EPR spectrum, could derive from an alteration in rate and/or amplitude of motion.

Layered Crystal Packing

The working model for *in meso* crystallogenesis posits that a lipid lamellar portal exists between the bulk cubic phase and the growth face of the crystal.[8] It serves as a conduit for protein molecules to migrate from the mesophase reservoir into the crystal. This aspect of the model is based, in part, on the observation that a layered packing prevails in crystals of membrane protein grown by the *in meso* method. The current study adds yet another piece of evidence in support of the hypothesis where BtuB molecules are arranged in stacked lamellae within the *in meso*-grown crystal (Figure 6(b)). Adjacent proteins within a layer have opposite orientations. This type of arrangement is consistent with a reconstitution process which introduces proteins with random orientation across the bilayer of the cubic phase. A summary of the layered packing observed with the different proteins that have been crystallized *in meso* is presented in Figure 10.

Membrane Boundary Location

The layered packing of membrane proteins observed with *in meso*-grown crystals likely comes about because proteins and lipids are free to move within the plane of the mesophase membrane from which crystallization occurs.[8,11] Such mobility allows for the transmembranal surface of proteins within a bilayer to come into direct contact with one another. This is in contrast to membrane proteins crystallized by the more traditional *in surfo* methods that can have a band of detergent around the protein preventing direct contact between transmembranal surfaces.[11] In *in meso*-grown crystals, the layered packing can be used to suggest limits to the transmembranal part of the protein. Assuming that contact between adjacent proteins within a layer arises because they have complementary hydrophobic surfaces, the region of overlap between them (see Figure 6(b)) must include the transmembranal part. In the case of BtuB, the overlap region is ~22 Å wide. However, it does not delineate the hydrophobic surface more specifically than that. To demark the transmembranal region more precisely requires additional analysis such as that based on transfer energy calculations (26; http://opm.phar.umich.edu/; Figure 3(b)). The latter indicates that the hydrophobic thickness of BtuB is 21.1 Å, the smallest value for any of the β–barrel proteins of known structure. This agrees well with the value obtained from the overlap analysis in Figure 6(b). The surface location of tryptophans and tyrosines in membrane proteins can also highlight the polar/apolar interface.[27] For BtuB, the tryptophan and tyrosine surface distribution (Figure 3(a)) is reasonably consistent with boundary locations identified by overlap and transfer energy calculations. The transmembranal region also corresponds well with a band of C_α-B-factor values in strands β3-β21 of the barrel that are everywhere less than 35 $Å^2$ (Figure 5(a)). Furthermore, the bulk of the lipid acyl chains are contained within the boundary locations as defined above (Figure 3(b)).

CONCLUSIONS

The structure of the vitamin B12 transporter BtuB has been solved to 1.95 Å using *in meso*-grown crystals. This represents the highest resolution to date for a β-barrel membrane protein with greater than 16 β-strands. It is also amongst the highest resolution structures for a membrane protein other than bacteriorhodopsin solved by the *in meso* method. Crystallization was done with functionally active protein reconstituted into the bilayer of the cubic phase. Functionality was demonstrated by substrate binding.

The overall structure of the protein is analogous to that of apo-BtuB crystallized by the detergent-based *in surfo* method. However, there are important differences that include 1) the N-terminal pentapeptide is present in the *in meso* structure but is not seen in the *in surfo* model, 2) residues 6 and 7 of the Ton box are rotated 180 degrees with respect to one another in the two structures, 3) the conformation of several extracellular loops extending from the barrel are very different in the two models, 4) the mobility, as judged by the average C_α-B-factor, is relatively low in the loop region of the *in meso* model, 5) protein is 1.2-times more densely packed in *in meso*-grown crystals, 6) a simple, layered arrangement of protein is observed in *in meso*-grown crystals in contrast to a more complex packing *in surfo*, and 7) lipids accompany the protein in the *in meso* structure while detergents are present in the *in surfo* model.

The *in meso* crystal structure is, in general, in good agreement with results reported in the literature obtained using SDSL and EPR. However, they are at variance in regard to the mobility characteristics of the N-terminal pentapeptide. The crystal structure shows this to be ordered despite having relatively high C_α-B-factor values. By contrast, the EPR study identifies these as 'natively disordered' residues regardless of ligand-binding status. It may be that mobility, as monitored by EPR, correlates with the crystallographic B-factor. The mobility characteristics of apo-BtuB, as judged by its average C_α-B-factor, is comparatively low in the *in meso* model. This has been attributed to a more densely packed crystal devoid of detergent micelles that are likely to support protein mobility.

There are four extracellular loops with markedly different conformations in *in meso* and *in surfo*-grown crystals of apo-BtuB. In one of these (loop 9–10), the loops point in opposite directions; into and out of the barrel. The others (loops 13–14, 15–16, 19–20) show disparate degrees and forms of tilting toward or away from the barrel lumen. Together these data paint a picture of a hydra-like protein consisting of a barrel with relatively static staves from which mobile loops of varying sizes extend reaching into the extracellular medium. The contrasting loop conformations captured in the *in meso* and *in surfo* structures described in this study illustrate the considerable flexibility in the ‘tentacles’ of this transport protein.

Layered crystal packing, which is emerging as a hallmark of membrane proteins crystallized *in meso*, has been used to identify the likely location of the lipid bilayer as it contacts the surface of the protein *in vivo*. In the case of BtuB, the apolar surfaces so defined are separated by just 21 Å. This value and the positioning of the polar/apolar boundaries are in good agreement with the distribution of lipids, surface tryptophans and tyrosines and with C_αB-factors in the protein model. They also match well the boundary locations defined by transfer free energy calculations.[26]

The high packing density observed with *in meso*-grown crystals may prove to be one of the methods enduring strengths. This should allow for higher diffraction quality with smaller crystals.

This work demonstrates that the *in meso* method works with targets that are other than compact bundles of transmembranal helices stabilized by chromophores. Our findings with apo-BtuB

suggest that the method has more general applicability and that it can be used to provide high-resolution structural data on colorless, β-barrel membrane proteins not buttressed by cofactors.

MATERIALS AND METHODS

Materials

Monoolein (M_r 356 g/mol, lot M-239-JA12-O) was purchased from Nu Chek Prep Inc. (Elysian, MN) and was used as received. 2,3-Dihydroxypropyl (7Z)-9,10-dibromooctadecanoate (bromo-MAG, M_r 516 g/mole, lots 180BR-10, 180BR-11 and 180BR-13) was received as a gift from Avanti Polar Lipids Inc. (Alabaster, AL). 2-Methyl-2,4-pentanediol (MPD, M_r 118.18 g/mol, lot 103K3655) and 2-[N-morpholino]ethanesulfonic acid hemisodium salt (MES, M_r 206.2 g/mol, lot 79F5615) were from Sigma (St. Louis, MO). Stock solution of 10 M ammonium formate was from Stock Options Salt Kit (HR2-245, lot 224504, Hampton Research, Aliso Viejo, CA). Cyanocobalamin (CNCbl, Vitamin B_{12}, M_r 1,355.4 g/mol, lot 062K14805) was received from Sigma. The following crystallization kits were used in this study: Crystal Screen HT (HR2-130, lot 213015-86-57), Index HT (HR2-134, lot 213404), SaltRX HT (HR2-136, lot 213605-05), MembFac (HR2-114, lot 211420) from Hampton Research, Aliso Viejo, CA; Wizard I & II (EBS-BWZ, lot EBS0000705200599) from Emerald BioSystems, Bainbridge Island, WA; MemStart (MD1-21USA, lot 003) from Molecular Dimensions Inc., Apopka, FL; JBScreen Membrane 1–3 (CS-306L, lot 2003/02) from Jena Bioscience GmbH, Jena, Germany. Water, with a resistivity of >18 MΩ·cm, was purified by using a Milli-Q Water System (Millipore Corporation, Bedford, MA) consisting of a carbon filter cartridge, two ion exchange filter cartridges, an organic removal cartridge and a final 0.22 μm filter.

The BtuB from *E. coli* was expressed in *E. coli* strain TNEO12 (pJC3) and purified as previously described[1,16] using 1.5 %(w/v) OG for extraction and 0.1 %(w/v) LDAO during purification. The solution of purified BtuB was prepared in 10 mM Tris/HCl pH 8.0, 0.1 M NaCl, 0.1 %(w/v) LDAO buffer. The concentration of BtuB was determined by light absorption at 280 nm using an extinction coefficient of 136,690 $M^{-1}cm^{-1}$ calculated from the aromatic amino acid content (28; http://ca.expasy.org/tools/protparam.html).

Methods

X-Ray Diffraction

Sample Preparation: Hydrated lipid samples were prepared at room temperature (between 19 and 25 °C) using a home-built mechanical syringe mixer[29,30] at 60 %(w/w) lyotrope and approximately 10 to 15 mg of lipid. Samples were loaded into 1 mm diameter glass or quartz capillaries (Hampton Research, Aliso Viejo, CA). The capillaries were flame-sealed using a propane/oxygen torch (Smith Equipment, Watertown, SD) and glued with ‘5 minute’ epoxy (Hardman Inc., Belleville, NJ).

Mesophase Diffraction: Nickel-filtered (0.02 mm thick) copper Kα x-rays (1.542 Å) from a rotating anode generator (RU-300, Rigaku USA Inc., Danvers, MA) were used to make low- and wide-angle powder diffraction measurements, as described.[31] The sample-to-detector distance, ~300 mm, was calibrated using silver behenate with a lamellar repeat (d_{001}) of 58.37 Å.[32] The samples were mounted in a temperature-controlled beryllium holder.[33]

Diffraction patterns were recorded on image plates (20 cm x 25 cm, Fuji HR-IIIN, Fuji Medical Systems USA, Stamford, CT). Exposed plates were scanned in a phosphor image scanner (Storm 840, Molecular Dynamics Inc., Sunnyvale, CA) at 100 μm resolution. The data was analyzed for d-spacing information using the program Fit2D, as described.[34]

Spectroscopy

UV-Visible Absorption: Spectra were recorded with a Uvikon XL dual beam spectrophotometer (Research Instruments Intl., San Diego, CA). Data was collected from 750 nm to 250 nm in 1 nm steps at 100 nm/min with air as the reference. The absorption spectrum of a lipid/lyotrope cubic phase dispersion or buffer alone in a 3 mm quartz cuvette (Hellma) recorded against air was subtracted from protein-containing sample spectra as appropriate. A flat-tipped 22-gauge needle (point style 3, inner diameter, 0.41 mm; outer diameter, 0.72 mm) was used to transfer the homogenous sample from the microsyringe mixing device to the cell. The loaded cell was capped with Parafilm and spun at 14,000 g for 10 min at room temperature.

Fluorescence: Emission spectra were recorded using an SFM3 fluorimeter (Bio-Logic Science Instruments, Claix, France) that included a 150-Watt Hg/Xe lamp (L2482, Hamamatsu, Japan) and Jobin Yvon monochromators (MM-200 driving unit, BH10 UV monochromators). 1 mm slits were placed at the entrances to and exits from the excitation and emission monochromators providing an 8 nm band pass. Light intensity was measured with a photomultiplier tube (Bio-Logic PMT 200) with an integration time of 100 ms.

Emission spectra from samples in 3 mm quartz cuvettes were recorded with an excitation wavelength of 305 nm. The latter was chosen to selectively excite tryptophan in the protein with minimal contribution from phenylalanine and tyrosine and to minimize photobleaching. Since 305 nm is on the red edge of the tryptophan absorption peak, possible inner filter effects are lessened. Additionally, this wavelength is close to a peak in the Hg/Xe lamp emission spectrum at 302 nm which provides for a stronger signal. Generally, emission spectra were recorded over a limited range from 360 to 320 nm (1 nm steps, 100 nm/min) to minimize bleaching. The inner filter correction was applied to all spectra, as described.[13]

Fluorescence Quenching: Quenching of tryptophan fluorescence by bromine labeled lipids (bromo-MAG) was used to demonstrate insertion of BtuB into the lipid bilayer of the cubic phase. For this purpose, bromo-MAG was mixed with molten monoolein at concentrations from 0 (pure monoolein) to 100 mol% (pure bromo-MAG) and the mixtures were used to prepare BtuB-containing cubic phase samples for fluorescence quenching measurements. That all bromo-MAG/monoolein mixtures form the cubic-Pn3m phase under conditions of measurement was confirmed by small-angle X-ray diffraction, as described.[13] Background correction was done using control samples with the same bromo-MAG/monoolein ratios that lacked BtuB.

Circular Dichroism: The conformation of apo-BtuB in micellar solution and reconstituted into the lipidic cubic phase was determined by circular dichroism (CD). Spectra were recorded using an AVIV Circular Dichroism Spectrometer (Model 202, Protein Solutions Inc. Lakewood, NJ) in the range from 250 nm to 190 nm in 1 nm steps with an equilibration time of 2 s per step. The bulk of the solution work was done using 1 mm path length quartz cuvettes. Because the monoolein samples have high background absorbances in the UV region, the CD spectra were noisy when collected using 1 mm cells. Accordingly, the bulk of the cubic phase data was acquired using either a 0.1 mm path length cuvettes which were loaded as described previously.[13] All measurements were made after a 1 h equilibration at 20 °C.

For the bulk of the spectroscopic measurements described above, samples were prepared and analyzed in triplicate.

CNCbl Binding—Binding of CNCbl to BtuB reconstituted into the fully hydrated cubic-Pn3m phase of monoolein was determined analogously to partitioning measurements, as described.[35] Briefly, a 30 mg bolus of BtuB-loaded cubic phase (60 %(w/w) monoolein, 40

%(w/w) lyotrope containing 15 mg BtuB/mL) was placed on the bottom of a semi-micro, UV-transparent, disposable cuvette (path length 1 cm; BrandTech Scientific, Essex, CT). To the cuvette was added 0.5 mL 67 μM CNCbl solution in 10 mM Tris-HCl buffer, pH 8.0. It was then capped and sealed with parafilm. Samples were shaken gently (Mistral Multi-Mixer) while being incubated at 20 °C. Binding was monitored as a decrease in absorption at 361 nm, the characteristic absorption maximum for CNCbl (extinction coefficient 27,500 $M^{-1}cm^{-1}$)[36] of the bathing solution. Equilibrium was reached after 5 d. Control samples containing CNCbl buffer with and without BtuB-free cubic phase did not reveal any appreciable change in the absorption at 361 nm over the 5 d period.

Binding was also quantified by monitoring ligand-induced intrinsic fluorescence quenching. For this purpose, the protein was first reconstituted into the cubic phase, as described above, using a solution consisting of apo-BtuB (0.6 mg protein/mL) in 0.1 %(w/v) LDAO, 0.1 M NaCl, 120 μM calcium chloride and 10 mM Tris-HCl buffer, pH 8.0. The cubic phase was then combined by mechanical mixing with a solution containing 0 – 10 μM CNCbl under conditions that ensured optical transparency. Fluorescence measurements were made as described above. Control data were collected with apo-BtuB in micellar solution, as described.[15] The dissociation constant, K_d, was calculated by Scatchard analysis. To this end, the fractional saturation of BtuB with ligand (η) was determined based on a normalized fluorescence. Normalization was done using fluorescence values recorded in the absence of ligand, and in the presence of saturating ligand concentration (100 μM). Free ligand concentration, $[CNCbl]_f$, was calculated based on the known total concentration of ligand and protein, and on η. A Scatchard plot of $\eta/[CNCbl]_f$ *vs.* η has an ordinate intercept of $1/K_d$ and a slope of $-1/K_d$ from which the binding constant is obtained. The extent of quenching observed upon ligand saturation was ~30% for protein dispersed in micellar solution and in the cubic phase.

Crystallization—*In meso* crystallization was performed with monoolein as the host lipid. The lipidic mesophase laden with protein was prepared as a 3/2 by volume mix of lipid and protein solution and dispensed into home-made 96-well crystallization plates using a home-built *in meso* crystallization robot.[37] A complete description of the sample preparation and dispensing procedure is available.[12,29,37] Trials were performed with 50 nL protein/lipid dispersion and 1 μL precipitant solution. Plates were incubated at 20 ºC for up to 30 d. Crystallization was monitored using an automatic imager (RockImager RI24, Formulatrix Inc., Waltham, MA) and manually by light microscope (Eclipse E400-POL, Nikon Inc., Melville, NY), as described.[37,38] Initial screening was performed using six 96-well blocks filled with precipitant solution from commercial crystallization kits (Crystal Screen HT, Index HT, SaltRx and MembFac from Hampton Research; Wizard I&II from Emerald BioSystems; MemStart from Molecular Dimensions and JBScreen Membrane from Jena Bioscience). Small crystals were found to form in the presence of MPD, pentaerythritol propoxylate (5/4 PO/OH), jeffamine M-600, 1,4-butanediol and KSCN. Conditions containing MPD were optimized using concentration-pH grid screens and different salts as additives to obtain ~100 μm-sized BtuB crystals. The best crystals were grown in 10–12 %(v/v) MPD, 0.1–0.2 M ammonium formate, 0.1 M MES, pH 6.5. Co-crystallization of BtuB with Ca^{2+} and with CNCbl/Ca^{2+} were attempted in which a BtuB solution was mixed with $CaCl_2$ or CNCbl/$CaCl_2$ solutions to yield final concentrations of 160 μM BtuB, 32 mM $CaCl_2$ and 210 μM CNCbl before mixing with monoolein. The same initial set of commercial crystallization screens as well as optimization screens used with apo-BtuB were employed in the co-crystallization trials.

Crystals of BtuB for crystallographic measurement were grown in a 72-well Nunc microbatch plate (HR3-122, Hampton Research, Laguna Niguel, CA). 200 nL lipid/protein dispersion was used in each well in conjunction with 3 μL precipitant solution. Wells were sealed with transparent tape (HR4-506, Manco Crystal Clear sealing tape, Hampton Research, Aliso Viejo, CA). Crystals grew to their full size (~100 x 60 x 25 μm^3) in 10–14 d. Harvesting was done

after 14 d using Hampton cryo-loops (0.1 mm diameter) and crystals were cryocooled and stored in liquid nitrogen. Lipidic cubic phase that had swollen in the presence of MPD and that had transformed into a sponge phase (see Preliminary Characterization section and Cherezov et al.[11]) had the consistency of a viscous liquid, which did not interfere with harvesting. MPD and lipid served as cryoprotectants and no additional cryoprotectant was used.

Crystallography—Diffraction measurements were performed on the F1 beamline at the Cornell High Energy Synchrotron Source (CHESS, Ithaca, NY) using a 100 μm diameter and 0.9124 Å wavelength beam, and an ADSC Quantum-4 detector. Crystals used for data collection measured approximately 100 x 60 x 25 μm^3. Several datasets were recorded at a sample-to-detector distance of 200 mm using a 0.5 ° or 1.0 ° oscillation and a 30 s exposure per image. The two best datasets were merged. Data reduction and scaling were performed with HKL2000.[39] The structure was solved by molecular replacement using 1NQE as a starting model. Refinement was done with REFMAC5 from the CCP4 suite.[40] Data collection and refinement statistics are summarized in Table 3. The Ramachandran plot shows that 93.4 % and 6.6 % of phi/psi angles are in favored and allowed regions, respectively.

Figures 3 and 5 through 10 were created using PyMol.[41]

Protein Data Bank accession number—Structure factors and coordinates have been submitted to the Protein Data Bank under the accession number – 2GUF.

Acknowledgements

MC thanks the members of his research group for invaluable input on this work. They include N. Hoefer, J. Lyons and Y. Misquitta. Grant support for MC was provided by Science Foundation Ireland (02-IN1-B266), the National Institutes of Health (GM61070 and GM75915) and the National Science Foundation (IIS-0308078), and for WAC by NIH GM-18457 and the Henry Koffler Professorship.

This work is based on research conducted at the Cornell High Energy Synchrotron Source (CHESS), which is supported by the National Science Foundation under award DMR 0225180, using the Macromolecular Diffraction at CHESS (MacCHESS) facility, supported by award RR-01646 from the National Institutes of Health, through its National Center for Research Resources.

References

1. Taylor R, Burgner JW, Clifton J, Cramer WA. Purification and characterization of monomeric Escherichia coli vitamin B12 receptor with high affinity for colicin E3. J Biol Chem 1998;273:31113–31118. [PubMed: 9813013]
2. Lazzaroni JC, Dubuisson JF, Vianney A. The Tol proteins of Escherichia coli and their involvement in the translocation of group A colicins. Biochimie 2002;84:391–397. [PubMed: 12423782]
3. Chimento DP, Mohanty AK, Kadner RJ, Wiener MC. Substrate-induced transmembrane signaling in the cobalamin transporter BtuB. Nat Struct Biol 2003;10:394–401. [PubMed: 12652322]
4. Fanucci GE, Lee JY, Cafiso DS. Spectroscopic evidence that osmolytes used in crystallization buffers inhibit a conformation change in a membrane protein. Biochemistry 2003;42:13106–13112. [PubMed: 14609320]
5. Fanucci GE, Coggshall KA, Cadieux N, Kim M, Kadner RJ, Cafiso DS. Substrate-induced conformational changes of the periplasmic N-terminus of an outer-membrane transporter by site-directed spin labeling. Biochemistry 2003;42:1391–1400. [PubMed: 12578351]
6. Fanucci GE, Cadieux N, Kadner RJ, Cafiso DS. Competing ligands stabilize alternate conformations of the energy coupling motif of a TonB-dependent outer membrane transporter. Proc Natl Acad Sci USA 2003;100:11382–11387. [PubMed: 13679579]
7. Landau EM, Rosenbusch JP. Lipidic cubic phases: a novel concept for the crystallization of membrane proteins. Proc Natl Acad Sci USA 1996;93:14532–14535. [PubMed: 8962086]
8. Caffrey M. Membrane protein crystallization. J Struct Biol 2003;142:108–132. [PubMed: 12718924]

9. Misquitta LV, Misquitta Y, Cherezov V, Slattery O, Mohan JM, Hart D, Zhalnina M, Cramer WA, Caffrey M. Membrane protein crystallization in lipidic mesophases with tailored bilayers. Structure 2004;12:2113–2124. [PubMed: 15576026]
10. Chimento DP, Mohanty AK, Kadner RJ, Wiener MC. Crystallization and initial X-ray diffraction of BtuB, the integral membrane cobalamin transporter of Escherichia coli. Acta Crystallog sect D 2003;59:509–511.
11. Cherezov V, Clogston J, Papiz MZ, Caffrey M. Room to Move: Crystallizing Membrane Proteins in Swollen Lipidic Mesophases. J Mol Biol 2006;357:1605–1618. [PubMed: 16490208]
12. Misquitta Y, Caffrey M. Detergents destabilize the cubic phase of monoolein: implications for membrane protein crystallization. Biophys J 2003;85:3084–3096. [PubMed: 14581209]
13. Liu W, Caffrey M. Gramicidin structure and disposition in highly curved membranes. J Struct Biol 2005;150:23–40. [PubMed: 15797727]
14. Bradbeer C, Reynolds PR, Bauler GM, Fernandez MT. A requirement for calcium in the transport of cobalamin across the outer membrane of Escherichia coli. J Biol Chem 1986;261:2520–2523. [PubMed: 3512539]
15. Banchs C, Wiener MC. A novel fluorescence assay for the measurement of cobalamin binding to the ourer membrane transporter BtuB. Poster abstract, Biophysical Society Meeting 2006:2568-Pos.
16. Kurisu G, Zakharov SD, Zhalnina MV, Bano S, Eroukova VY, Rokitskaya TI, Antonenko YN, Wiener MC, Cramer WA. The structure of BtuB with bound colicin E3 R-domain implies a translocon. Nat Struct Biol 2003;10:948–954. [PubMed: 14528295]
17. Blundell, TL.; Johnson, LN. Protein Crystallography. Academic Press; New York: 1976.
18. Shultis DD, Purdy MD, Banchs CN, Wiener MC. Outer membrane active transport: structure of the BtuB:TonB complex. Science 2006;312:1396–1399. [PubMed: 16741124]
19. Pawelek PD, Croteau N, Ng-Thow-Hing C, Khursigara CM, Moiseeva N, Allaire M, Coulton JW. Structure of TonB in complex with FhuA, E.coli outer membrane receptor. Science 2006;312:1399–1402. [PubMed: 16741125]
20. Briggs J, Chung H, Caffrey M. The temperature-composition phase diagram and mesophase structure characterization of the monoolein/water system. J Phys II France 1996;6:723–751.
21. Kolbe M, Besir H, Essen LO, Oesterhelt D. Structure of the light-driven chloride pump halorhodopsin at 1.8 A resolution. Science 2000;288:1390–1396. [PubMed: 10827943]
22. Xu Q, Axelrod HL, Abresch EC, Paddock ML, Okamura MY, Feher G. X-Ray structure determination of three mutants of the bacterial photosynthetic reaction centers from Rb. sphaeroides; altered proton transfer pathways. Structure 2004;12:703–715. [PubMed: 15062092]
23. Bond PJ, Sansom MS. Membrane protein dynamics versus environment: simulations of OmpA in a micelle and in a bilayer. J Mol Biol 2003;329:1035–1053. [PubMed: 12798692]
24. Dickerson RE, Goodsell DS, Neidle S. the tyranny of the lattice. Proc Natl Acad Sci USA 1994;91:3579–3583. [PubMed: 8170950]
25. McHaourab HS, Lietzow MA, Hideg K, Hubbell WL. Motion of spin-labeled side chains in T4 lysozyme. Correlation with protein structure and dynamics. Biochemistry 1996;35:7692–7704. [PubMed: 8672470]
26. Lomize MA, Lomize AL, Pogozheva ID, Mosberg HI. OPM: orientations of proteins in membranes database. Bioinformatics 2006;22:623–625. [PubMed: 16397007]
27. White SH, Wimley WC. Membrane protein folding and stability: physical principles. Annu Rev Biophys Biomol Struct 1999;28:319–365. [PubMed: 10410805]
28. Gasteiger, E.; Hoogland, C.; Gattiker, A.; Duvaud, S.; Wilkins, MR.; Appel, RD.; Bairoch, A. Protein Identification and Analysis Tools on the ExPASy Server. In: Walker, JM., editor. The Proteomics Protocols Handbook. Humana Press; 2005. p. 571-607.
29. Cheng A, Hummel B, Qiu H, Caffrey M. A simple mechanical mixer for small viscous lipid-containing samples. Chem Phys Lipids 1998;95:11–21. [PubMed: 9807807]
30. Qiu H, Caffrey M. Lyotropic and thermotropic phase behavior of hydrated monoacylglycerols: structure characterization of monovaccenin. J Phys Chem B 1998;102:4819–4829.

31. Cherezov V, Qiu H, Pector V, Vandenbranden M, Ruysschaert JM, Caffrey M. Biophysical and transfection studies of the diC(14)-amidine/DNA complex. Biophys J 2002;82:3105–3117. [PubMed: 12023234]
32. Blanton TN, Huang TC, Toraya H, Hubbard CR, Robie SB, Louer D, Gobel HE, Will G, Gilles R, Raftery T. JCPDS-International Centre for diffraction data round robin study of silver behenate. A possible low-angle X-ray diffraction calibration standard. Powder Diffr 1995;10:91–95.
33. Briggs J, Caffrey M. The temperature-composition phase diagram and mesophase structure characterization of monopentadecenoin in water. Biophys J 1994;67:1594–1602. [PubMed: 7819491]
34. Misquitta Y, Caffrey M. Rational design of lipid molecular structure: a case study involving the C19:1c10 monoacylglycerol. Biophys J 2001;81:1047–1058. [PubMed: 11463646]
35. Clogston J, Caffrey M. Controlling release from the lipidic cubic phase. Amino acids, peptides, proteins and nucleic acids. J Control Release 2005;107:97–111. [PubMed: 15990192]
36. Hill JA, Pratt JM, Williams RJP. The chemistry of vitamin B12. Part I. The valency and spectrum of the coenzyme. J Chem Soc (London) 1964:5149–5153.
37. Cherezov V, Peddi A, Muthusubramaniam L, Zheng YF, Caffrey M. A robotic system for crystallizing membrane and soluble proteins in lipidic mesophases. Acta Crystallog sect D 2004;60:1795–1807.
38. Cherezov V, Caffrey M. Nano-volume plates with excellent optical properties for fast, inexpensive crystallization screening of membrane proteins. J Appl Cryst 2003;36:1372–1377.
39. Otwinowski Z, Minor W. Processing of X-ray diffraction data collected in oscillation mode. Methods Enzymol 1997;276:307–326.
40. Collaborative Computational Project Number 4. The CCP4 suite: programs for protein crystallography. Acta Crystallog sect D 1994;50:760–763.
41. DeLano, WL. The PyMol molecular graphic system. DeLano Scientific; San Carlos, CA, USA: 2002.
42. Kabsch W, Sander C. Dictionary of protein secondary structure: pattern recognition of hydrogen-bonded and geometrical features. Biopolymers 1983;22:2577–2637. [PubMed: 6667333]
43. Chimento DP, Kadner RJ, Wiener MC. Comparative structural analysis of TonB-dependent outer membrane transporters: implications for the transport cycle. Proteins 2005;59:240–251. [PubMed: 15739205]

Abbreviations

bromo-MAG
: 2,3-dihydroxypropyl(7Z)-9,10-dibromooctadecanoate

BtuB
: outer membrane cobalamin transporter

CD
: circular dichroism

CHESS
: Cornell High Energy Synchrotron Source

CNCbl
: cyanocobalamin (vitamin B_{12})

EPR
: electron paramagnetic resonance

LH2
: light harvesting complex II

MPD
: 2-methyl-2,4-pentanediol

RMSD

root mean square distance

SDSL

site-directed spin labeling

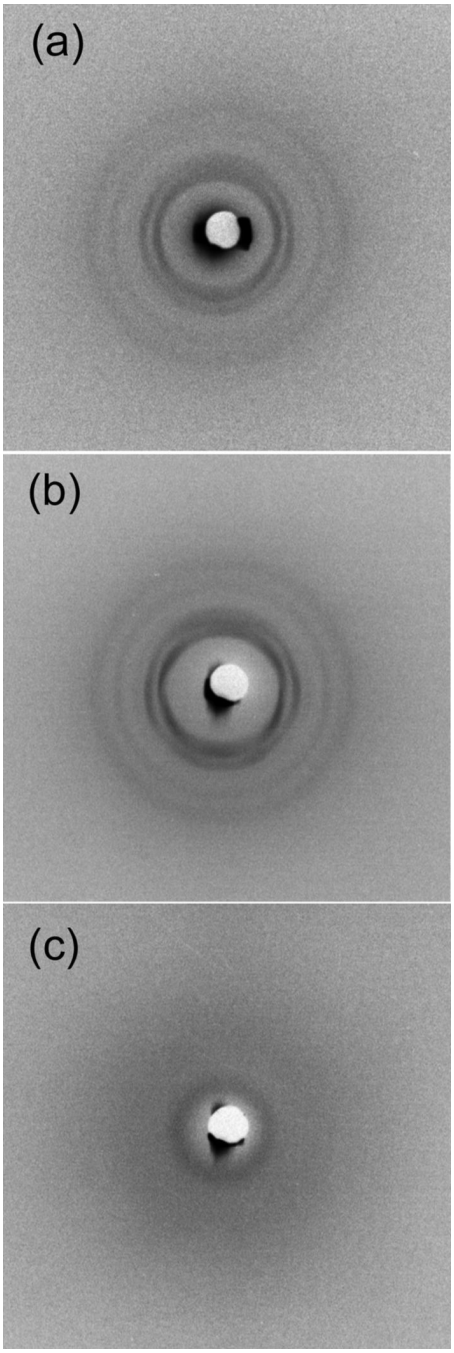

Figure 1.

Small-angle X-ray diffraction patterns of hydrated monoolein prepared with water (a), apo-BtuB protein solution (b), and apo-BtuB protein solution followed by incubation with MPD-containing precipitant for 16 days at 20 °C (c). The cubic-Pn3m phase with lattice parameters of 104.8 Å and 104.3 Å was recorded in (a) and (b), respectively. The diffuse ring surrounding the beam stop shadow in (c) is characteristic of the L3 or sponge phase. It has a d-spacing of 95 Å corresponding to a cubic-Pn3m phase with a lattice parameter of 150 Å assuming that the first two reflections (110 and 111) broaden and merge upon moving to lower angles with increasing MPD concentration, as described.[11] Samples were prepared with 60 %(w/w) monoolein and 40 %(w/w) water in (a), 60 %(w/w) monoolein and 40 %(w/w) protein solution

(12.9 mg BtuB/mL in 20 mM Tris/HCl pH 8.0, 0.1 M NaCl, 0.1 %(w/v) LDAO) in (b) and (c). In (c) 2 μL of the lipid/protein mesophase in an X-ray capillary tube was overlain with 10 μL of precipitant solution containing 10 %(v/v) MPD, 0.2 M ammonium formate, 50 mM MES pH 6.5 and incubated for 16 days at 20 °C before data collection. Micro-crystals of BtuB were present in (c) at the end of the incubation period.

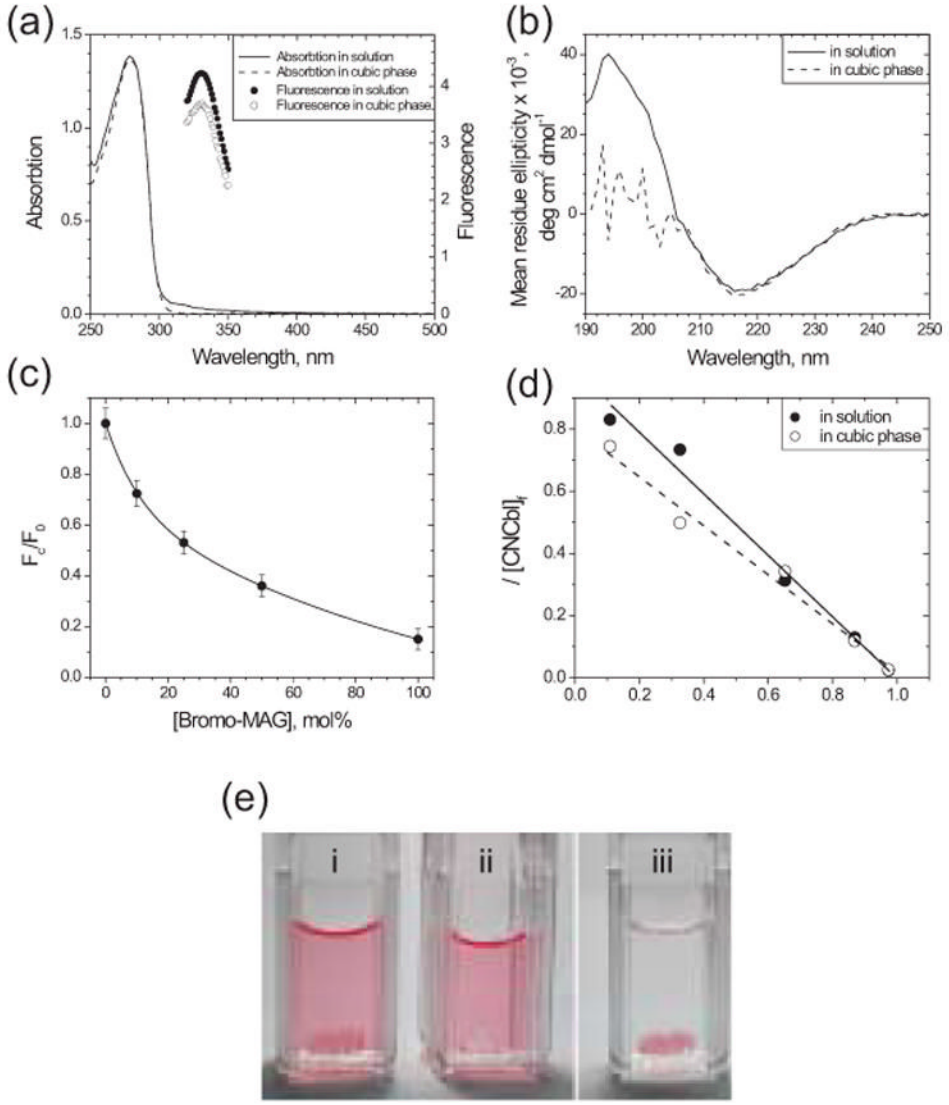

Figure 2.

Spectrophotometric and visual properties of BtuB in detergent solution and in the cubic phase. **(**a**)** UV-visible absorption and fluorescence emission spectra of apo-BtuB in detergent solution and in the cubic-Pn3m phase. **(b)** CD spectra of apo-BtuB in detergent solution and in the cubic phase. The region of the cubic phase spectrum below ~208 nm is not reliable because of strong background absorption by the lipid, as described.[13] **(**c**)** Quenching of apo-BtuB intrinsic fluorescence by bromo-MAG in the cubic phase of hydrated monoolein. Fluorescence intensity (F_c) was normalized to the value recorded in the absence of quenching lipid (F_0). Values reported are the average of at least triplicate sample preparations. **(**d**)** Scatchard analysis for the binding of CNCbl to apo-BtuB in micellar solution (solid circles) and in the cubic phase of hydrated monoolein (open circles). The corresponding dissociation constant, K_d, values are 1.02 and 1.24 nM. See Methods for details. **(e)** Photograph of a bolus of cubic phase with (i, iii) and without (ii) reconstituted apo-BtuB equilibrated for 6 days at 20 °C with a solution of 67 μM CNCbl. In (iii), the bathing CNCbl solution was replaced with CNCbl-free buffer just before the photograph was taken to make the labeling of the bolus more obvious. The bolus of cubic phase can be seen as an elliptically shaped object at the bottom of a cuvette.

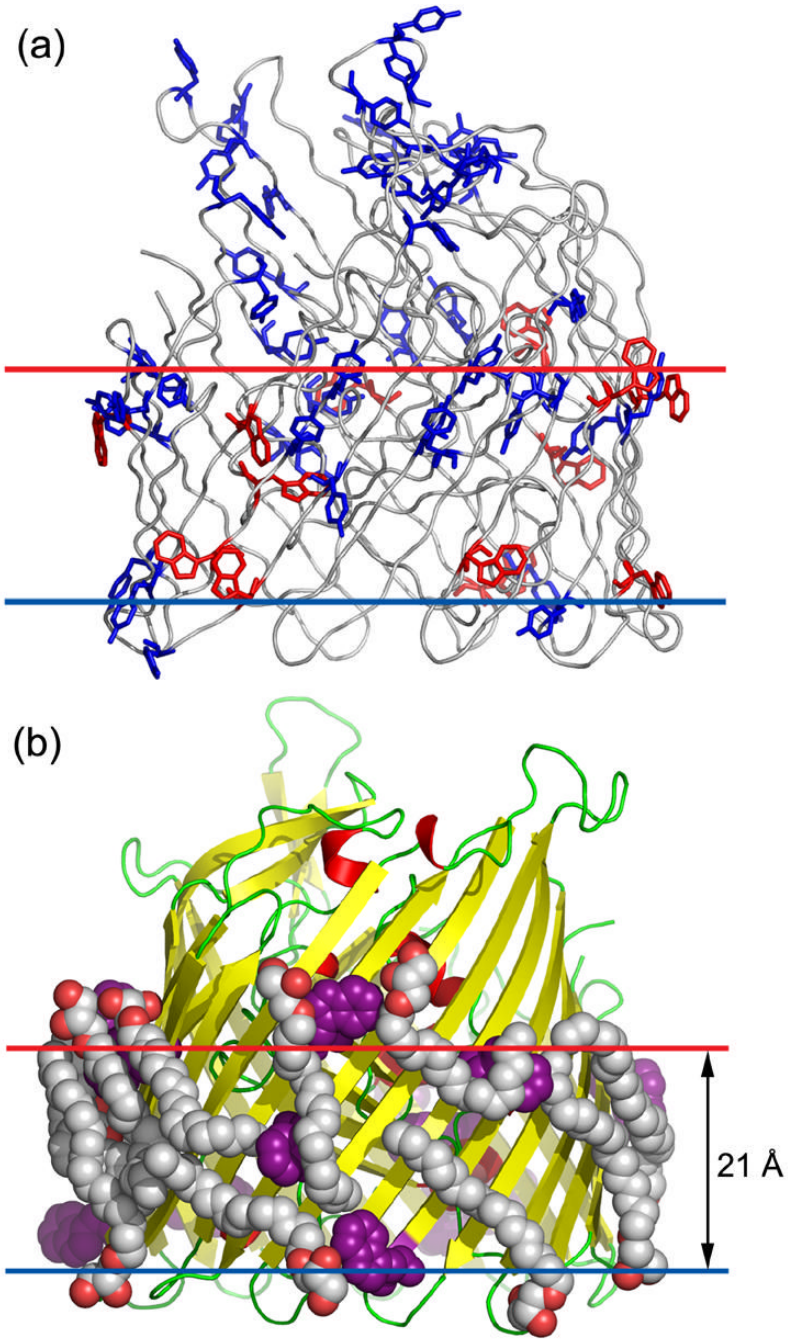

Figure 3.

The hydrophobic boundaries of apo-BtuB as defined by the distribution of tryptophans, tyrosines, and lipids in the model, and by transfer free energy calculations.[26] **(a)** Distribution of tryptophans (red) and tyrosines (blue) in apo-BtuB. The hydrophobic boundaries referred to in the text are shown as horizontal lines spaced approximately 22 Å apart. The backbone is shown in transparent grey so that all tryptophans and tyrosines in the protein can be seen clearly. **(b)** Cartoon representation of secondary structure elements (α-helix, red; β-strand, yellow) in the apo-BtuB model with boundaries located based on transfer free energy calculations. Tryptophans (purple) and lipids (carbon, grey; oxygen, red) are shown in van der Waals sphere

representation. The blue and red horizontal lines in (a) and (b) represent the periplasmic and extracellular membrane boundaries, respectively.

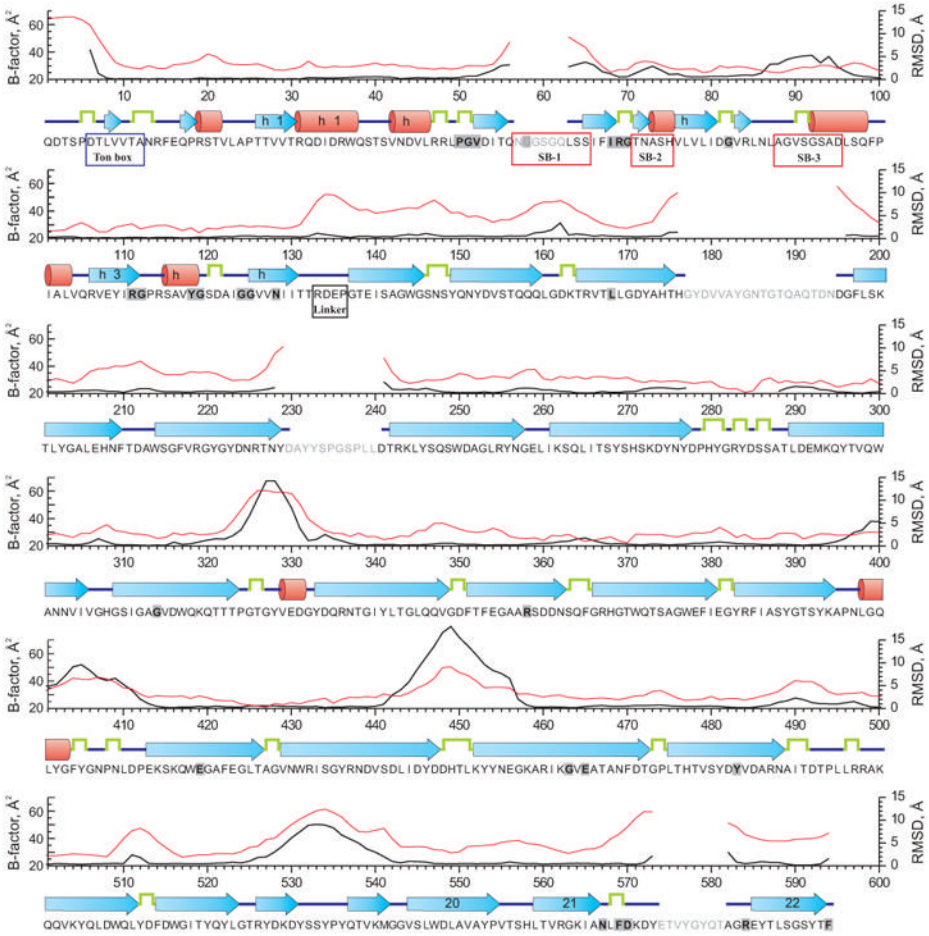

Figure 4.

Sequence, secondary structure and C_α-B-factor (red line) of apo-BtuB and the C_α-RMSD between the *in meso* (this work) and the *in surfo* (1NQE) models (black line). Secondary structure assignment was done using DSSP.[42] A gray font is used to represent residues that were not resolved in the *in meso* model. A grey shaded box and bold font are used to identify conserved amino acids.[43] The Ton box, substrate binding loops, and linker are enclosed in blue, red and black boxes, respectively. Blue arrows, red cylinders and green detour lines represent β-strands, α-helices and turns, respectively.

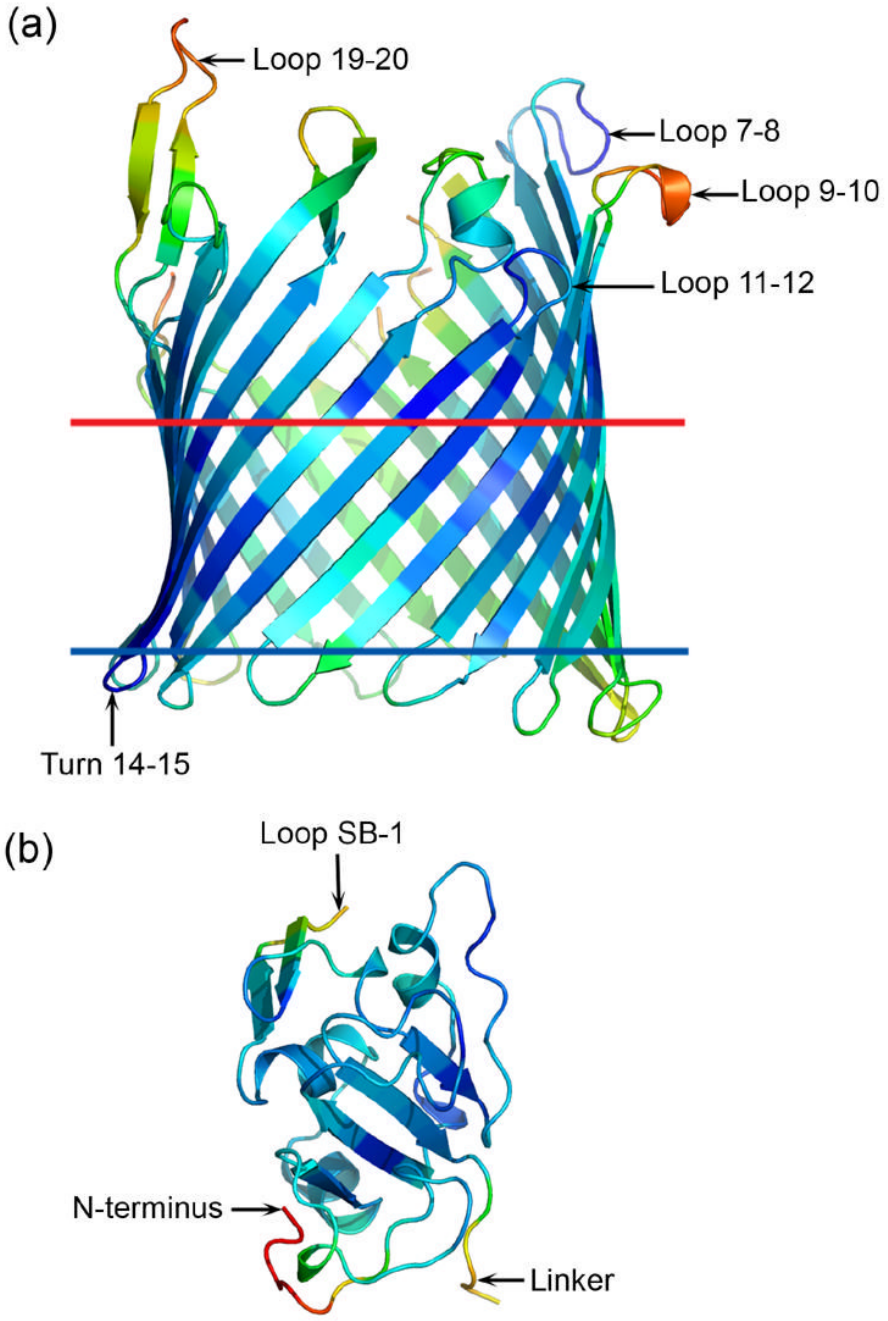

Figure 5.

Cartoon representation of the barrel (a) and hatch (b) domains of apo-BtuB rainbow color-coded according to C_{α}-B-factor value. In this model the highest (red) and lowest (blue) B-factor values are 65.6 and 20.9 Å ^{2}, respectively. The various parts of the protein referred to in the text are labeled. The relative orientation of the hatch with respect to the barrel domain is as in the intact protein. The hydrophobic boundaries referred to in the text are shown as horizontal lines (blue and red for periplasmic and extracellular sides, respectively) spaced approximately 22 Å apart.

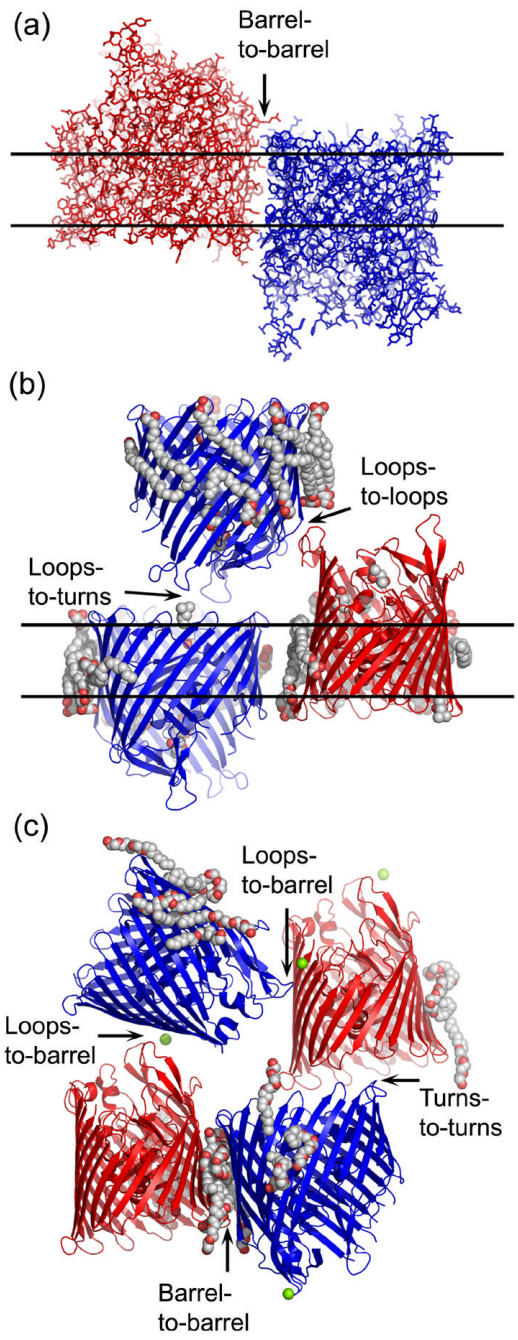

Figure 6.

Contacts in apo-BtuB crystals grown by the *in meso* ((a) and (b), this work) and *in surfo* ((c), 1NQE) methods. (a) In-plane barrel-to-barrel contacts. Lipid molecules are removed to expose direct protein-protein contacts. (b) Stacking loops-to-loops and loops-to-turns interactions. Parts of the model involved in contacts referred to in the text are labeled. The blue and red protein coloring denotes molecules with opposite polar orientation.

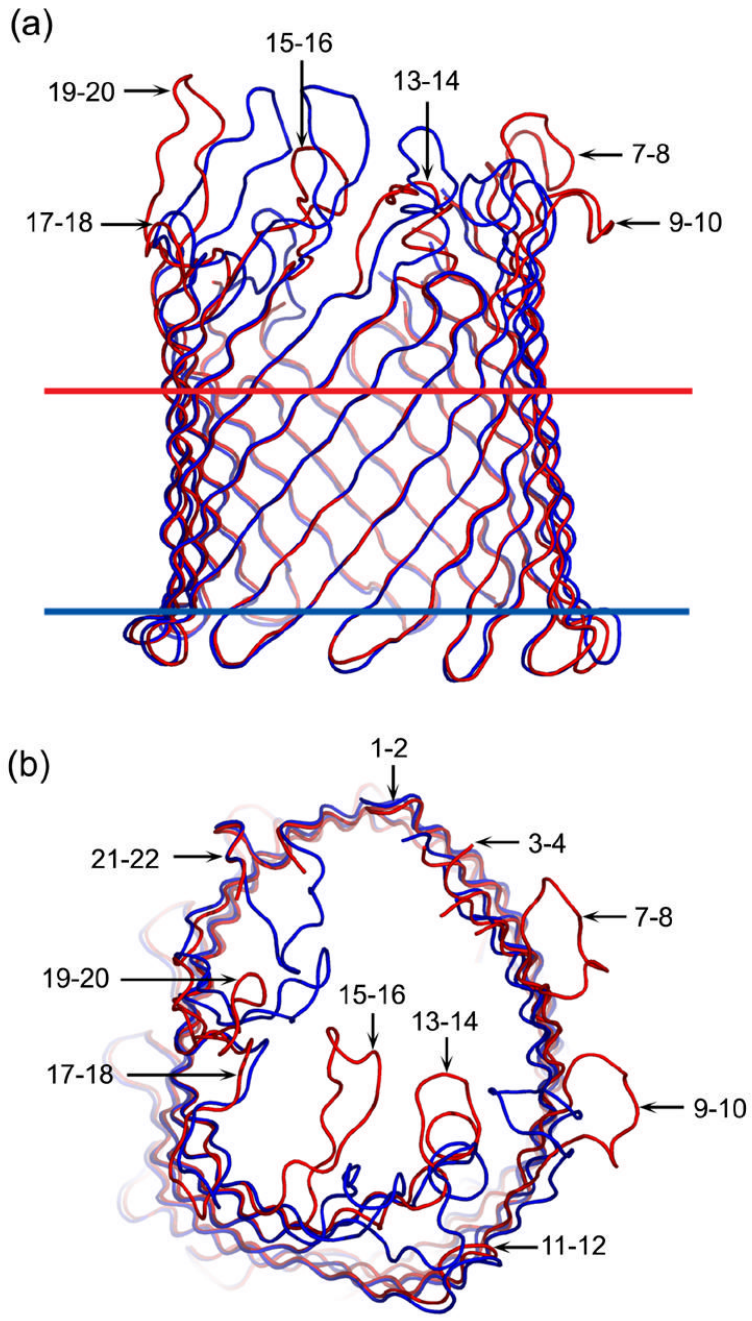

Figure 7.
Comparison of the extracellular loop region in apo-BtuB crystallized *in meso* (red, this work) and *in surfo* (blue, 1NQE) viewed from within the plane of the membrane (a) and from the extracellular space (b). Individual loops are labeled as described in the text. The hatch domain is omitted for clarity. The hydrophobic boundaries referred to in the text are shown as horizontal lines (blue and red for periplasmic and extracellular sides, respectively) spaced approximately 22 Å apart.

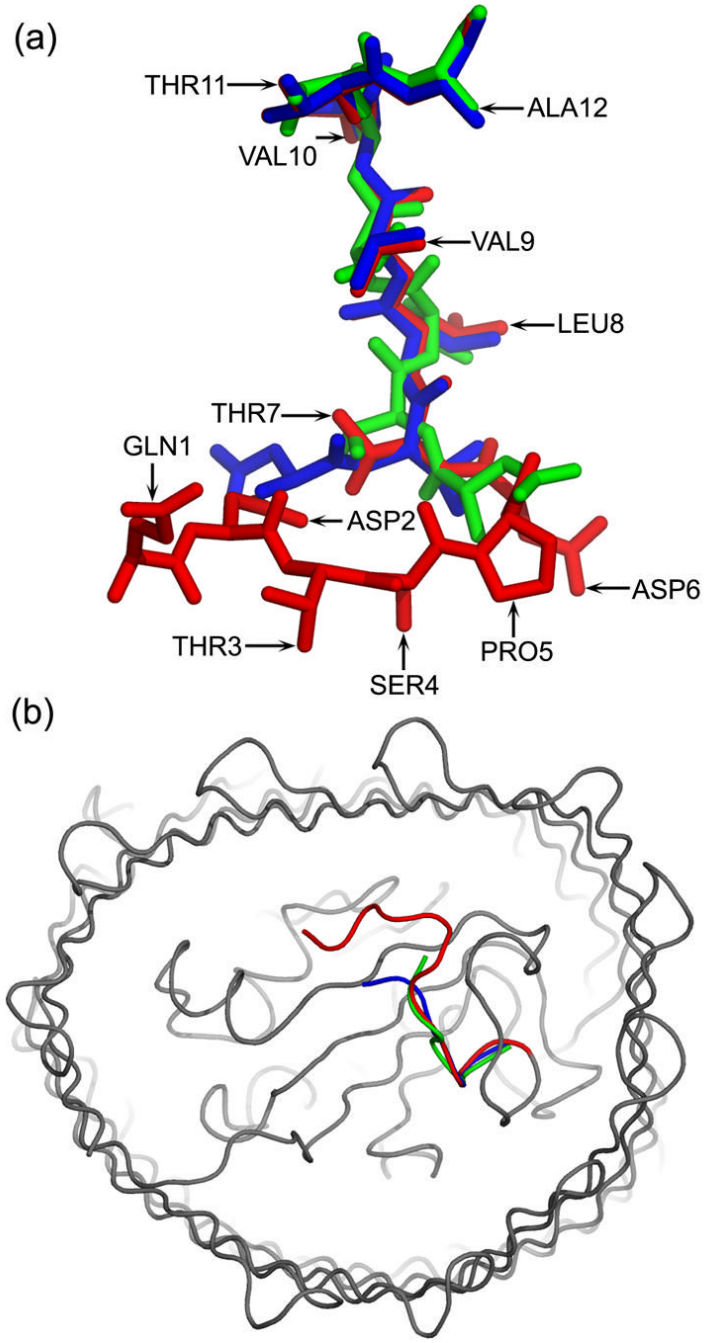

Figure 8.

Comparison of the N-terminal dodecapeptide (a) in apo-BtuB (b) crystallized *in meso* (red and grey, this work) and *in surfo* (blue, 1NQE), and in the BtuB-CNCbl complex crystallized *in surfo* (green, 1NQH). The Ton box is in the N-terminal dodecapeptide and extends from residue 6 to 12. The relative orientations of the N-terminal residues in (a) and (b) are different and were chosen to facilitate comparisons among the three models. Residues are identified by name and sequence position in (a). The view in (b) is from the periplasm.

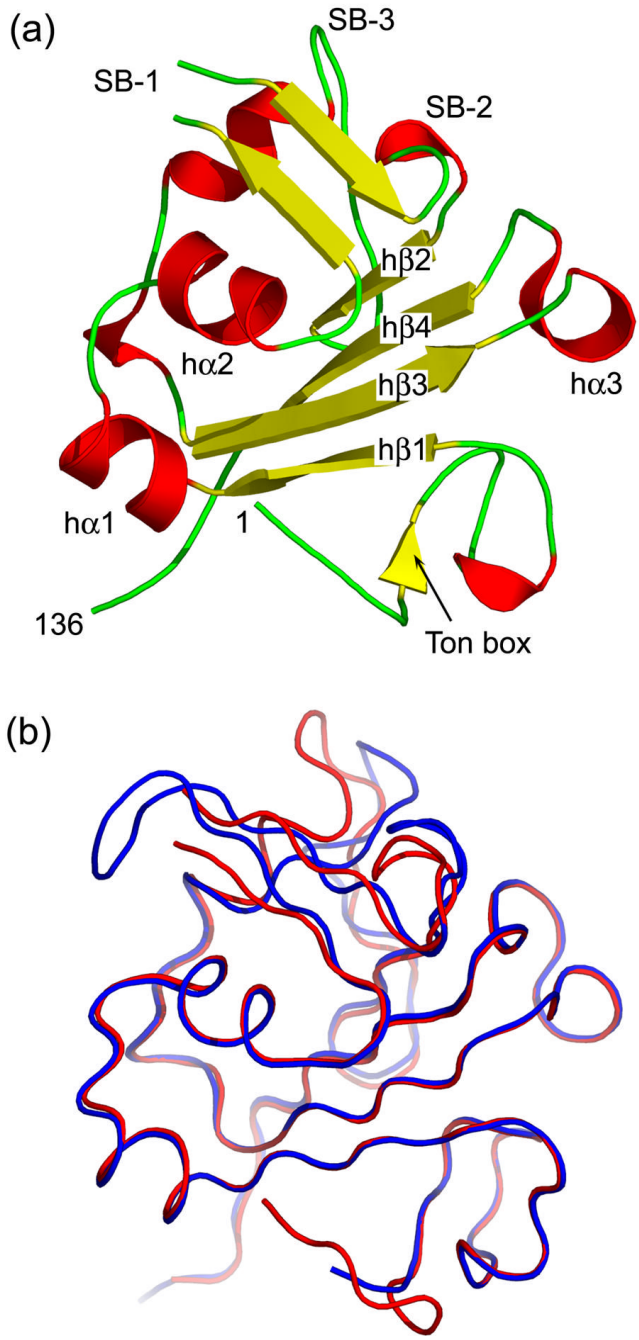

Figure 9.
Cartoon representation of the secondary structure in the hatch domain (residues 1–136) of apo-BtuB (a) and a comparison of the hatch domain structure in apo-BtuB obtained using *in meso*- (red, this work) and *in surfo*- (blue, 1NQE) grown crystals (b). Parts of the domain referred to in the text are labeled in (a). Residues 57 to 62 in the substrate binding loop 1 (SB-1) are disordered and are not included in the *in meso* model. The orientation of the hatch domains are the same in (a) and (b).

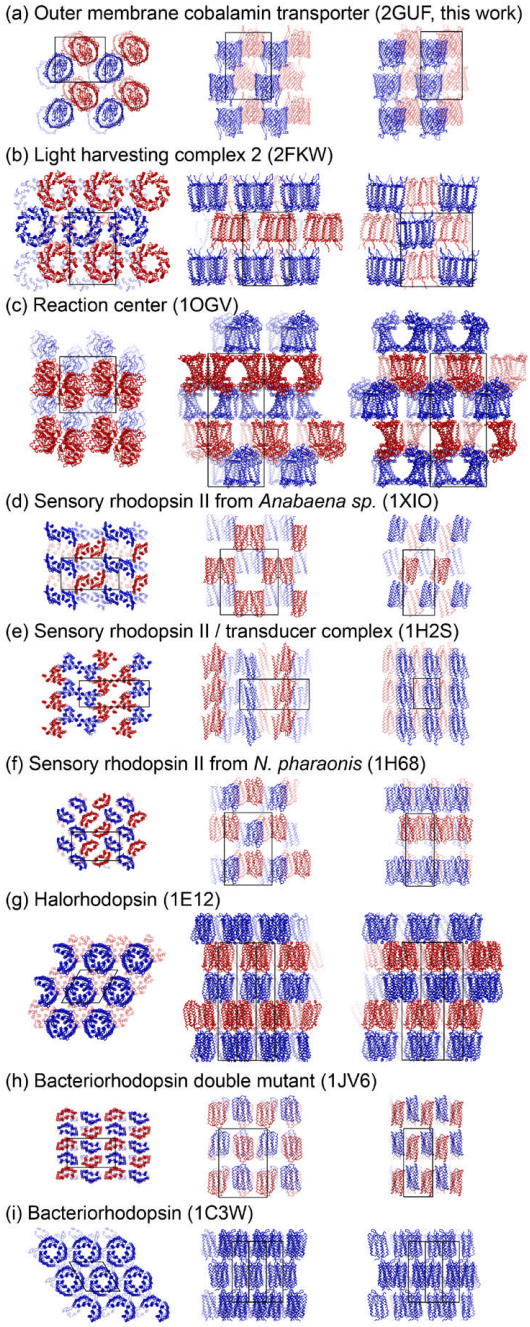

Figure 10.

A comparison of the packing arrangement in crystals of membrane proteins grown by the *in meso* method. The blue and red denotes proteins with opposite polar orientation. The view on the left in each panel represents a projection along the stacking axis. The views in the center and on the right are from within the plane of the stacked lamellae along the two other unit cell axes. Black outlines represent projections of the unit cell. Proteins are identified by name and PDB accession number.

Table 1

Backbone root mean squared differences (Å) between BtuB models[a] obtained using crystals grown *in meso* and *in surfo* with and without bound calcium, calcium and CNCbl, and the colicin R135 peptide.

		in surfo		
	apo-	**+Ca^{2+}**	**+Ca^{2+} + CNCbl**	**+R135**
in meso				
apo-	2.87	2.86	2.57	2.59
in surfo				
apo-		0.34	0.76	0.74
+Ca^{2+}			0.79	0.90
+Ca^{2+} + CNCbl				1.05

[a] The PDB accession codes are: *in meso* apo-, 2GUF; *in surfo* apo-, 1NQE; *in surfo* + calcium, 1NQG; *in surfo* + calcium + CNCbl, 1NQH; *in surfo* + R135, 1UJW

Table 2

A comparison of the properties of membrane protein crystals grown by the *in meso* and *in surfo* methods. [a]

Name	PDB ID	Mw, kDa	Space group	Resol., Å	a, Å	b, Å	c, Å	R	R_{free}	Solv. %	V_m, Å^3/Da	Mean B, Å^2
In meso												
BtuB	2GUF	66.4	P 21 21 21	1.95	72.61	80.88	118.68	0.189	0.225	53.1	2.62	38.7
LH2	2FKW	92.4[b]	P 21 21 21	2.45	82.86	126.56	131.03	0.186	0.254	55.6	2.80	31
RC	1OGV	92.8[b]	P 42 21 2	2.35	99.97	99.97	237.19	0.214	0.244	55.6	2.80	40.3
SR II from *Anabaena sp.*	1XIO	30.2[b]	C 2 2 21	2.00	103.1	116.51	56.19	0.230	0.256	56.0	2.79	21.9
SR II/transducer	1H2S	24.1/5.7[b]	P 21 21 2	1.93	124.3	46.96	53.84	0.226	0.258	53.4	2.64	32.4
SR II from *N. pharaonis*	1H68	25.4[b]	C 2 2 21	2.10	84.83	128.74	50.74	0.237	0.256	54.9	2.73	37.5
hR	1E12	27[b]	P 63 2 2	1.80	67.3	67.3	209.2	0.237	0.257	51.4	2.53	32.5
bR double mutant	1JV6	26.9[b]	C 2 2 21	2.00	51.8	121.3	85.7	0.244	0.240	52.1	2.60	N/A
bR	1C3W	24.4[b]	P 63	1.55	60.63	60.63	108.16	0.158	0.225	53.2	2.65	N/A
In surfo												
BtuB	1NQE	66.4	P 31 2 1	2.00	81.59	81.59	210.08	0.196	0.232	59.5	3.04	41.2
LH2	1NKZ	92.4[b]	H 3 2	2.00	117.05	117.05	298.44	0.170	0.190	69.4	4.05	23
RC	1RZH	93.8[b]	P 31 2 1	1.80	139.35	139.35	184.96	0.221	0.233	76.0	5.20	28
bR	1BRR	26.8[b]	C 1 2 1	2.90	120.52	105.96	80.19	0.256	0.299	54.0	2.67	58.2

[a] Values were obtained from the corresponding record in the PDB

[b] Values are for a chromophore-free protein

Table 3

Data collection and refinement statistics

A. *Data Collection*	
Space group	$P2_12_12_1$
Unit-cell parameters (Å)	a =72.61, b = 80.88, c = 118.68
Mosaicity (°)	0.5
Resolution limits (Å)	50 – 1.95 (2.02 – 1.95)[a]
Total reflections	275,371
Unique reflections	51,400
Rejected reflections (%)	0.2
Redundancy	5.4 (4.8)[a]
Completeness (%)	98.7 (94.3)[a]
I/σ	20.0 (3.6)[a]
R_{merge} (%)	7.9 (41.9)[a]
B. *Refinement*	
Refinement resolution (Å)	40 – 1.95
R-factor (%)	18.9
R_{free}[b] (%)	22.5
Number of reflections	48,447
RMSD bond length (Å)	0.019
RMS bond angles (°)	2.01
Correlation Coefficient	0.96
ML coordinate error (Å)	0.096
Number of atoms	5,054

[a] Numbers in parentheses refer to the highest resolution shell

[b] R_{free} was calculated using 5.1% of data randomly excluded from refinement